2022 IEEE International Symposium on
Safety, Security, and Rescue Robotics (SSRR)
November 8-10, 2022. Seville, Spain

Progressive Series-Elastic Actuation with Magnet-based Non-linear Elastic Elements

Boi Okken, Stefano Stramigioli, and Wesley Roozing

***Abstract*— We present the design and development of a non-linear series-elastic element based on repelling magnets. Progressive stiffness offers the transparency advantages of a low-stiffness elastic actuator at low load levels, and the high torque tracking bandwidth of a high-stiffness actuator at high loads. The design space of this magnet-based concept is thoroughly analysed, for both box- and arc-segment magnets. A proof-of-concept prototype is presented which is experimentally validated. A gain-scheduled torque controller is used to exploit its non-linear dynamics. Simulation and experimental results demonstrate the viability of the concept.**

I. Introduction

Robotic actuation developments in the last two decades have shown a trend away from stiff, highly-geared, position-controlled drives to torque- and impedance-controlled systems aimed at physical interaction performance. Series elastic actuators (SEAs) [1]–[3] combine the torque capacity of geared drives with low output impedance, and exhibit excellent interaction performance.

Selection of the series stiffness presents a trade-off between torque tracking bandwidth and actuator transparency (or low output impedance) [3], [4]. Research into overcoming this trade-off has focused on non-constant or adjustable stiffness of the elastic element. The two primary approaches in this area are Variable Stiffness Actuators (VSAs) and Non-linear Series-Elastic Actuators (NSEAs). VSAs [5], [6] use a secondary motor to adjust the physical stiffness. This leads to increased mechanical complexity, and the solutions are generally relatively bulky. Conversely, in NSEAs the elasticity is passively non-linear [7]–[18]. By increasing stiffness with deflection (progressive stiffness) they can provide higher torque resolution and higher safety at low output torque, while offering a higher "bandwidth" than a traditional constant-stiffness SEA with similar deflection and torque resolution at higher output torque. This is similar to mammalian muscles [19], [20], which also progressively increase their stiffness with force output.

Existing NSEAs can be divided into three main categories: 1) mechanism-based, 2) material-based, and 3) magnetism-based. The first deflects a linear elastic element through a non-linear mechanism [7]–[12] or uses structure controlled stiffness [12], [13]. Second, material-based NSEAs use the inherent non-linear properties of materials to generate non-linear stiffness [14], [15]. However, existing materials with these properties tend to suffer from high hysteresis. Lastly, magnetism-based NSEAs are based on the non-linear repelling force of magnets [16]–[18].

The authors are with the Robotics & Mechatronics (RaM) group, University of Twente, The Netherlands. E-mail: {b.okken,s.stramigioli,w.roozing} at utwente.nl.

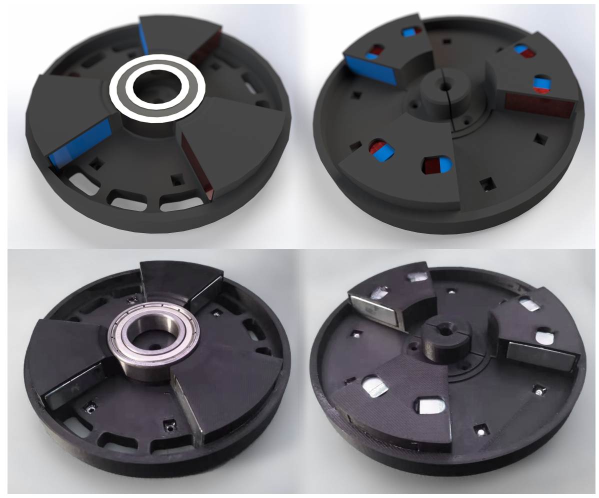

Fig. 1: Magnet-based elastic element: CAD and realised prototype.

This work presents a magnet-based concept for non-linear series-elastic elements, with a rotational design similar to the recent work [18]. Contrary to [18] however, we thoroughly analyse the design space of such elements for two types of magnets, leading to design guidelines and an analytical model able to predict torque and stiffness of a design. We then present a proof-of-concept prototype to validate the concept (Fig. 1). We characterise the prototype's non-linear stiffness profile, and finally evaluate closed loop control performance in both simulation and experiment. The contributions of this paper are summarised as follows:

1) A non-linear elastic element concept based on box- or arc-segment magnets, including design guidelines;
2) An analytical model based on empirical magnet repelling force data that predicts torque and stiffness curves for a given design;
3) A proof-of-concept prototype that validates the concept and shows a stiffness range of 3x;
4) A suitable gain-scheduled torque controller that significantly outperforms linear controllers in NSEAs.

This paper is organized as follows. First, Sec. II considers the design parameters and analysis of magnet-based non-linear elastic elements. Sec. III presents the proof-of-concept prototype, together with its torque/stiffness characterisation. Sec. IV then proceeds to design the gain-scheduled torque controller. Simulation and experimental results are reported in Sec. V and Sec. VI, respectively. Finally, Sections VII and VIII discuss the results and conclude the work.

2022 IEEE International Symposium on Safety, Security, and Rescue Robotics (SSRR) | 978-1-6654-5680-7/22/$31.00 ©2022 IEEE | DOI: 10.1109/SSRR56537.2022.10018635

II. Concept and Analysis

A. Principle of operation

In this work the desired non-linear stiffness is generated with the use of magnets. Following their inherently non-linear repelling force, the force imposed on each magnet increases progressively as distance between a pair of magnets decreases. Rotational movement of electrical motors implies a radial orientation of the magnets. Therefore, the concept shown in Figs. 1 and 2 comprises of two halves that fit together as inner hub and outer hub. In Fig. 2, α_{max} represents the maximum deflection range in one direction that the two halves of the element can move with respect to each other, β denotes the angular space that an individual magnet segment can occupy, and $N \geq 1$ is the total number of segments on each half (leading to $2N$ opposing magnet pairs).

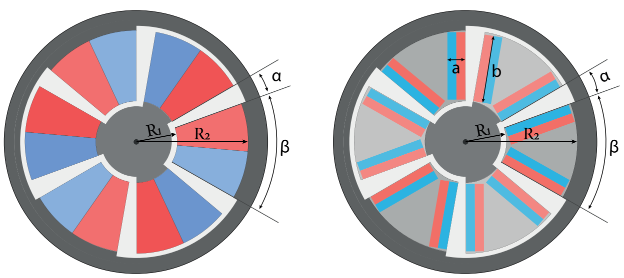

(a) Arc-segment magnets. **(b)** Box magnets.

Fig. 2: Elastic elements with different types of magnets and $N = 3$. Different magnet types are discussed in Sec. II-B.2.

B. Design parameters

1) Deflection range, torque, and stiffness: In this section we consider the effect of the design parameters on deflection range, torque range, and stiffness range. We start with deflection range. The geometry shown in Fig. 2a results in a trade-off between angular magnet space β_{max} and the achievable deflection α_{max}:

$$\beta_{\text{max}} = \frac{\pi}{N} - \alpha_{\text{max}}. \tag{1}$$

Computing Eq. (1) yields Fig. 3, which shows the usable angular magnet space β_{max} for a required deflection range α_{max} and number of magnet segments N. For a given (minimum) deflection range, a vertical line can be drawn which intersects with the lines of different values of N. Indicated in the figure are the chosen design parameters for the presented prototype, with a deflection of $\alpha_{\text{max}} = 10\,°$, N=3 (presented in Sec. III-A).

Fig. 4 shows torque and stiffness as function of deflection α, for fixed β and different number of segments N (i.e. α_{max} varies as in Fig. 3). The analytical model to compute these results will be presented in Sec. II-C. Fig. 4 shows that an increase in magnet segments (given constant β effectively increasing total magnet volume) increases maximum torque τ_{max}, base stiffness k_0 (at $\alpha = 0$), and maximum stiffness,

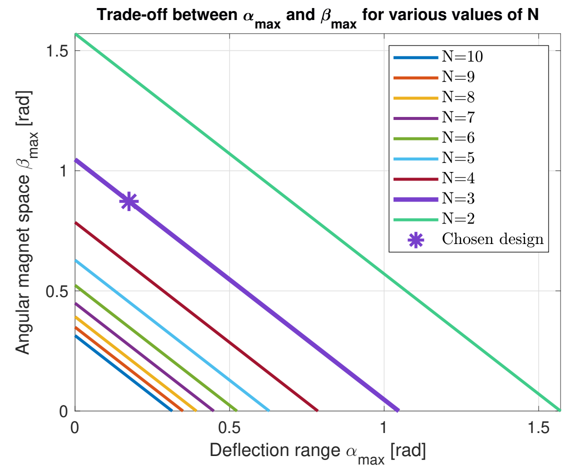

Fig. 3: Trade-off between α_{max} and β for various values of N.

at the cost of deflection range α_{max} (Fig. 3). The increase in base stiffness is a result of the non-linear nature of the repelling force: smaller distance between magnets at $\alpha = 0$ leads to an increased force gradient between each pair, and thus increased base stiffness. Lastly, notice that for a

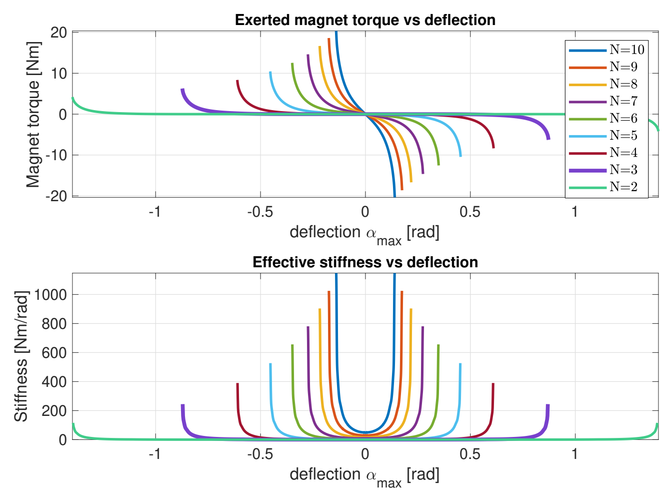

Fig. 4: Effect of N on deflection range α_{max}, torque, and stiffness. Example magnet of 30x2.6x12 mm, and $\beta_{\text{max}} = 10\,°$, $R_2 = 60$ mm.

given deflection range α_{max} and number of segments N, total angular space utilised by magnets results from (1) as

$$\beta_{\text{total}} = N\,\beta = \pi - N\,\alpha_{\text{max}}, \tag{2}$$

which is maximised for small N, due to fewer 'gaps' needed for deflection. Hence, peak torque and stiffness in a given volume are also maximised for small[1] N. To conclude, to maximise torque and stiffness in a given volume:

1) Set the maximum deflection range α_{max} to the minimal required for the application, and large enough to achieve satisfactory base stiffness k_0;
2) Minimise the number of segments N;

[1]It should be noted however that for very small values (e.g. $N \in \{1, 2\}$) the majority of repelling force is not oriented perpendicular to the axis of rotation, and hence internal stresses increase and torque and stiffness reduce.

both of which maximise total magnet area β_{total}. Some iteration may be required given the available magnets. Further guidelines on outer dimensions (volume) are presented in Sec. II-B.3.

2) Magnet type: So far we have discussed *circumferentially polarized arc segment magnets* shown in Fig. 2a, which maximise surface utilisation for a given arc β and respective inner and outer radii R_1 and R_2. However, compared to regular 'box' type magnets, they are more expensive and are generally not available as off-the-shelf components. Therefore, the prototype realised in this work will utilize box magnets, as shown in Fig. 2b. Although this reduces torque and stiffness capacity, the principle of operation remains unchanged. Following their rectangular shape, the thickness a relative to length b of box magnets represents an additional parameter that can be optimised to maximise surface utilisation. Given an outer radius R_2, arc β, and magnet length b, its maximum thickness a that does not intersect the other magnet in the arc is given by

$$a = (R_2 - b)\,\tan\left(\frac{\beta}{2}\right)\ . \tag{3}$$

The maximum surface area ab (and thus volume) can then be derived as $b = \frac{R_2}{2}$. Notice that this is independent of both β and N. It should be noted that a maximum surface utilization does not necessarily imply neither maximum torque nor stiffness; to maximise these properties, numerical iteration using available magnets is necessary. However, maximum surface utilisation typically yields a design very close to maximum torque and stiffness.

3) Outer radius R_2: An increase in outer radius R_2, and thus overall size, increases both maximum torque and stiffness. This is because 1) magnet area scales with radius (progressively for arc-segment magnets), and 2) a larger radius increases moment arm. Therefore, R_2 has a relatively large impact. This can be seen in Fig. 5, for box and arc-segment magnets respectively. The arc-segment magnets in Fig. 5b have a constant inner radius R_1 of 24 mm (for the central hub and bearing).

Tables I and II lists different values for outer radius R_2, resulting total magnet volume, peak torque, base stiffness, as well as torque density and stiffness density, given a 12 mm thickness. For box magnets, torque and stiffness density decrease with outer radius, as effective space utilisation decreases. Arc-segment magnets fully utilise the additional area, and thus torque and stiffness density remain almost constant. Secondly, they are approximately 2.5-6.2x and 2.1-3.6x higher, respectively, than for box magnets.

Lastly, increasing the thickness of the elastic element linearly increases its generated torque. This makes it trivial to scale a design for different torque and stiffness capacity.

C. Elastic element model

Traditionally, analysing the repelling force of magnets is analytically impossible and computationally expensive. It can be approximated by using empirical data available from magnet manufacturers and resellers, or experimentally

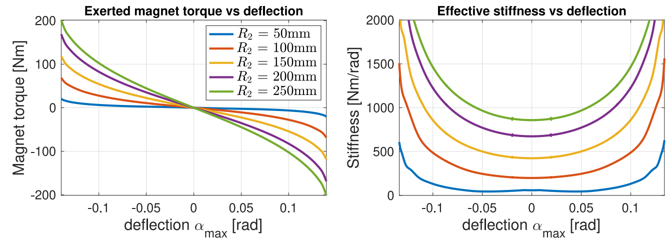

(a) Box magnets: $R_1 = \frac{R_2}{2}$ mm.

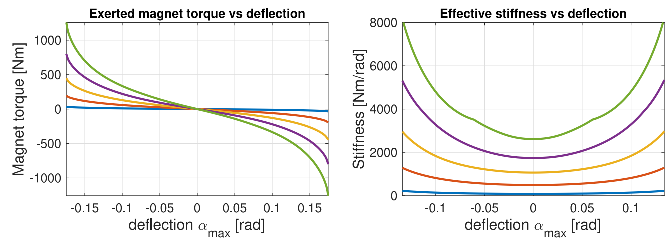

(b) Arc-segment magnets: $R_1 = 24$ mm.

Fig. 5: Effect of R_2 on torque and stiffness. $\beta = 10°$, $N = 10$.

R_2 [mm]	M. vol. [mm^3]	τ_{max} [Nm]	k_0 [$\frac{\text{Nm}}{\text{rad}}$]	τ dens. [$\frac{\text{Nm}}{\text{mm}^3}$]	k dens. [$\frac{\text{Nm}}{\text{rad}\cdot\text{mm}^3}$]
50	6.5e2	20	58	$2.12e-4$	$6.16e-4$
100	2.6e3	68	198	$1.80e-4$	$5.25e-4$
150	5.9e3	118	424	$1.39e-4$	$5.00e-4$
200	1.1e4	168	674	$1.11e-4$	$4.47e-4$
250	1.6e4	201	856	$8.54e-5$	$3.63e-4$

TABLE I: Box magnets and results used in Fig. 5a.

R_2 [mm]	M. vol. [mm^3]	τ_{max} [Nm]	k_0 [$\frac{\text{Nm}}{\text{rad}}$]	τ dens. [$\frac{\text{Nm}}{\text{mm}^3}$]	k dens. [$\frac{\text{Nm}}{\text{rad}\cdot\text{mm}^3}$]
50	2.0e3	33	85	$3.58e-4$	$9.00e-4$
100	9.8e3	194	491	$5.15e-4$	$1.30e-3$
150	2.3e4	446	1.0e3	$5.26e-4$	$1.26e-3$
200	4.1e4	800	1.7e3	$5.30e-4$	$1.15e-3$
250	6.5e4	1.2e3	2.6e3	$5.33e-4$	$1.11e-3$

TABLE II: Arc magnets and results used in Fig. 5b.

obtained data (e.g. Fig. 6, data from K&J Magnetics Inc.[2]). This data can be obtained by measuring the force between two parallel magnets with a varying linear distance. We use the empirical data to obtain the most accurate result for the real-world elastic element.

To derive the generated torque as function of deflection angle, we proceed as follows. First, note that the magnet surfaces are not parallel (only at $\alpha = \alpha_{max}$). This means that the distance between two magnets is a function of both radius r and deflection angle α. To account for this, the magnet is divided into infinitesimally small slices along the radial direction (Fig. 7). Each slice is then treated as a fraction of the original magnet in terms of force (and through radius, torque). Integrating radially and multiplying by number of magnet pairs then yields the torque of the elastic element as

[2]K&J Magnetics Inc., *Magnet repelling force data for box-type magnets*, https://www.kjmagnetics.com/calculator.repel.asp, Feb 2021.

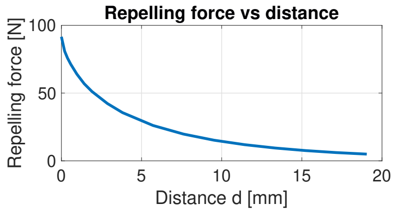

Fig. 6: Empirical repelling force for the selected N52 30x12x12 mm magnet.

function of deflection angle. For both box and arc-segment type magnets this results in:

$$\tau_{\text{box}}(\alpha) = \frac{N}{R_2 - R_1} \int_{R_1}^{R_2} r\, F_{\text{box}}(d(\alpha, r))\, \mathrm{d}r, \tag{4}$$

$$\tau_{\text{arc}}(\alpha) = \frac{4\,N}{R_2^2 - R_1^2} \int_{R_1}^{R_2} r^2\, F_{\text{arc}}(d(\alpha, r))\, \mathrm{d}r, \tag{5}$$

where $F_\bullet$ denotes empirical magnet force data as function of linear distance, which is given by

$$d(\alpha, r) = 2\,r \sin\left(\frac{\alpha_{\max} - \alpha}{2}\right). \tag{6}$$

Stiffness is then computed as the derivative with respect to the deflection angle: $k(\alpha) = \frac{\mathrm{d}\tau(\alpha)}{\mathrm{d}\alpha}$.

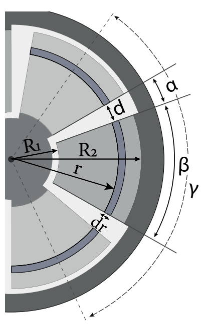

Fig. 7: Modelling magnet torque using infinitesimal slices.

III. Non-linear elastic element prototype

A. Design requirements and chosen parameters

For the prototype, a torque range of ± 10 Nm, base stiffness of at least 20 Nm/rad, and deflection range of at least $\alpha_{\max} = 10^\circ$ are desired. Using Eq. (1), this results in $\beta = 50^\circ$ for $N = 3$. Design iteration with available magnets yields a chosen box magnet of 30x12x12 mm. Following Eq. (3), this results in an inner radius $R_1 = 30$ mm and an outer radius $R_2 = 60$ mm. The magnet grade used is N52. Using online available magnet data scaled to the quoted maximum repelling strength (Fig. 6), together with Eq. (4), yields the torque and stiffness curves shown in Fig. 8. The chosen box magnets satisfy the design requirements, with ± 11.3 Nm peak torque, base stiffness of 32 Nm/rad, and peak stiffness over 150 Nm/rad. Secondly, Fig. 8 also shows an arc-segment magnet based design with comparable torque and stiffness ranges, which has an outer radius R_2 of only 40 mm.

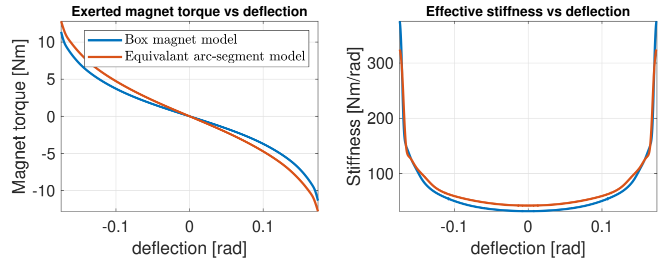

Fig. 8: Torque and stiffness predictions for 1) 30x12x12 mm box magnets, and 2) a comparable arc-segment magnet design.

For comparison, an arc-segment magnet design of dimensions similar to the box magnet design ($R_2 = 63$ mm) would produce peak torque of 50 Nm and peak stiffness of $>$1000 Nm/rad; approximately 4.5x and 3x higher than the box magnet based design, respectively.

B. CAD and prototype

Fig. 1 shows both the CAD model and the realised elastic element prototype. Fig. 9 shows a section view of the elastic element. For illustration, the upper half is coloured in black, the lower in light grey. This shows how the two elastic element halves fit together, including the bearings in white, and magnets in blue.

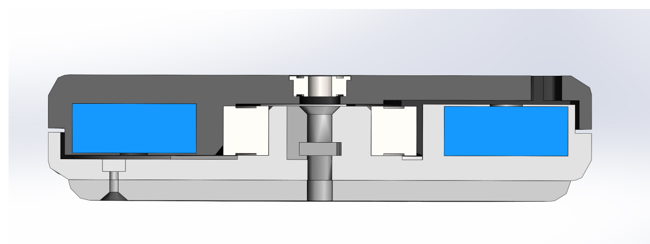

Fig. 9: Section view showing both halves in black and white, respectively. Bearings shown in white, magnets in blue.

For construction of the prototype, 3D printing was selected. It should be noted that the presented magnet-based non-linear elastic element is less mechanically complex than traditional NSEA and VSA designs and thus relatively simple and inexpensive to produce. Carbon fiber filled nylon was selected for its physical properties; it has comparatively high mechanical toughness and ability to resist peak forces in the design. The prototype's mass is 672 g including magnets. Measurements on the prototype are done using a load cell (*HTC-Sensor TAL220*[3,4]) on a lever arm, connected to a development board (*NXP/Freescale Frdm K64F*). The data are further processed on a PC. As control, an *ATI Industrial Mini-40* force/torque (F/T) sensor is used to confirm the load-cell measurements are linear with torque.

C. Static characterisation

We first characterise the deflection-torque profile of the realised prototype by static tests. These results are subsequently validated against the analytical model derived in

[3]Sparkfun Electronics, load cell - 10kg, straight bar (tal220).
[4]Sparkfun Electronics, load cell amplifier (hx711).

Sec. II-C. The test setup fixes the elastic element (optionally through the F/T sensor) and allows it to be deflected in one degree increments through a pointer which integrates the load cell. The measured bending moment is proportional to the torque produced by the element. The designed and manufactured test setup can be seen in Fig. 10.

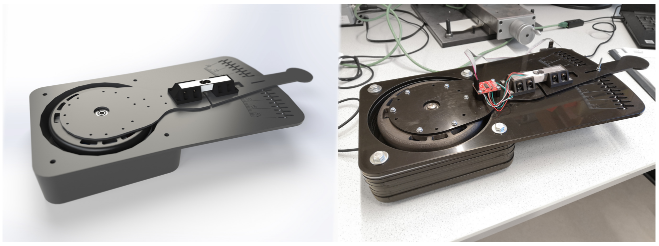

Fig. 10: CAD and the manufactured static test setup.

Fig. 11 shows the torque and stiffness results of the prototype, as well as a polynomial fit (in red). Secondly, the torque and stiffness predicted by the model are shown (in yellow). The results show strong agreement between the model and data in terms of torque, and desired torque range of $\pm 10\,\mathrm{Nm}$ is achieved. The peak stiffness towards maximum deflection is however significantly lower; stiffness varies from approximately 40 to 120 Nm/rad. This range of 3x is competitive when compared to other designs [12], [18]. Additionally, our prototype achieves significantly higher torque per unit volume by more effective space utilisation.

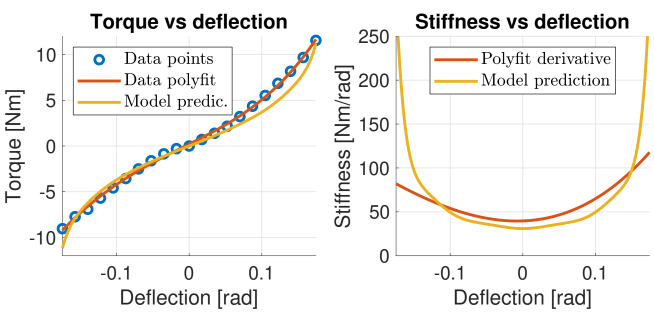

Fig. 11: Static characterisation: Torque and stiffness profiles compared to model predictions.

IV. Torque control

A. Series-Elastic Actuator model

We model a series-elastic actuator based on the magnet-based elastic element using the model shown in Fig. 12. It comprises a motor and gearbox with torque $\tau_{\mathrm{m}} = g_{\mathrm{m}}\, i$, inertia I_{m}, friction R_{m}, and gear ratio n. The gearbox output is coupled to the output q through the non-linear elastic element, with deflection $\alpha = n^{-1}\,\theta - q$. Its apparent stiffness is given by $k(\alpha)$, parameterized using the analytical model described in Sec. II-C. Following the use of magnets, we consider the internal friction of the elastic element to be negligible. For static testing of the element, the output of the actuator is considered to be fixed ($q \equiv 0$). The dynamics are then given by

$$I_{\mathrm{m}}\,\ddot{\theta} = \tau_{\mathrm{m}} - n^{-1}\,\tau - R_{\mathrm{m}}\,\dot{\theta}, \tag{7}$$

where the elastic element torque $\tau(\alpha)$ is given by a polynomial approximation, of either Eq. (4) or (5). From this we also define $k(\alpha)$, to denote the apparent stiffness as function of deflection.

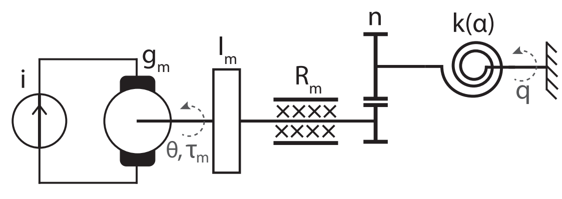

Fig. 12: IPM of the actuator with the output fixed ($q \equiv 0$).

For control purposes we also define a linear model with fixed stiffness $\bar{k}$, written in terms of torque:

$$\begin{bmatrix} \dot{\tau} \\ \ddot{\tau} \end{bmatrix} = \begin{bmatrix} 0 & 1 \\ -\frac{\bar{k}}{I_{\mathrm{m}}\, n^2} & -\frac{R_{\mathrm{m}}}{I_{\mathrm{m}}} \end{bmatrix} \begin{bmatrix} \tau \\ \dot{\tau} \end{bmatrix} + \begin{bmatrix} 0 \\ \frac{\bar{k}}{I_{\mathrm{m}}\, n} \end{bmatrix} \tau_{\mathrm{m}} \tag{8}$$

B. Control concept

Given a torque measurement, a linear torque controller could be used on an actuator incorporating the non-linear elastic element. However, as will be shown later, due to the strong non-linearity no single linear controller can provide sufficient performance over the full operating range. We tackle this issue using gain scheduling; adapting the control gains on-line based on a linearisation around the current operating point. An advantage of using gain scheduling is the ability to exploit standard linear time invariant control techniques to design this non-linear controller.The dominant source of non-linearity is the non-linear stiffness. Hence, given a characterisation of its deflection-stiffness properties (Fig. 11), a measurement of its deflection may be used as the exogenous scheduling variable.

C. Gain-scheduled full state feedback

Fig. 13 shows the proposed gain-scheduled state feedback controller, with torque reference τ^*. The feedback gains N_1, N_2 denote the proportional and derivative gains on torque respectively. They are derived using traditional linear quadratic regulator (LQR) methods for each stiffness operating point. M_1, M_2 denote the scheduling as function of the current stiffness estimate $\hat{k}(\alpha)$, derived from measured deflection α. Similarly, $\hat{\tau}(\alpha)$ denotes the torque estimate.

N_1, N_2 are derived using the linear model (8), with $\bar{k} \in [30, 300]$ (i.e. the dynamic stiffness range of the model), and $Q = \mathrm{diag}(1, 7\mathrm{e}-5)$ and $R = 5\mathrm{e}-2$. The resulting stiffness-dependent gains are shown in Fig. 14. The proportional torque feedback gain N_1 remains constant, however the derivative torque feedback reduces with increased stiffness, following the change in the plant's natural damping ratio. For quick computation we use a fractional fit for $N_2 = M_2(\hat{k})$, shown as red dashed line in Fig. 14. The feed-forward gain N_{FF} is used to achieve zero steady state error:

$$N_{\mathrm{FF}} = N_1 + g_{\mathrm{m}}^{-1} n^{-1}\,. \tag{9}$$

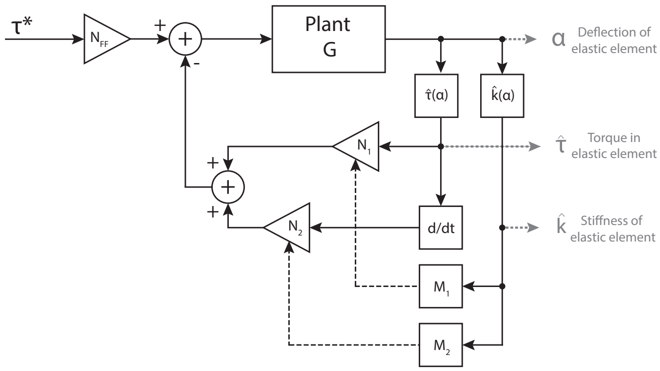

Fig. 13: Overview of the proposed gain-scheduled controller.

Notice that N_{FF} depends only on constants, and more importantly, is independent of stiffness.

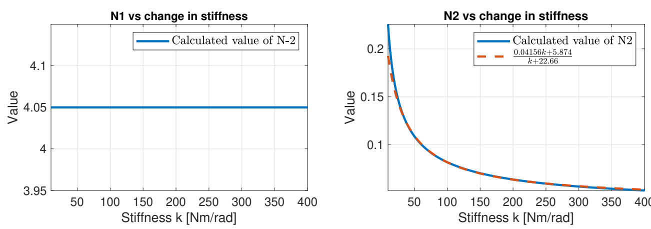

Fig. 14: LQR feedback gains N_1 and N_2 over fixed stiffness $\bar{k}$.

V. Simulated results

In this section we present simulation results that demonstrate the following:

1) The gain-scheduled controller outperforms linear controllers throughout the stiffness range;
2) Non-linear (progressive) stiffness allows to combine benefits of low stiffness during low-force (transparent) interaction with the benefits of high stiffness during large torque tracking [3].

The simulations are performed with the parameters of the physical system, which are listed in Table III. The motor/gearbox combination comprises a Maxon EC60 flat motor[5,6] and GP52C 43:1 gearbox[7].

Parameter	Value	Unit
Torque constant g	$5.25\text{e}-2$	Nm/A
Motor/gear friction R_m	$1.5\text{e}-4$	Ns/m
Motor inertia I_m	$8.32\text{e}-5$	kg m^2
Gearbox ratio n	43	-

TABLE III: Physical system parameters.

A. Controller comparison: Step response

We first compare the gain-scheduling controller to linear controllers tuned for either low (30 Nm/rad) or high (300 Nm/rad) stiffness, through step responses. Figs. 15a to 15c show the response in the low-stiffness region (low torque), middle of the stiffness region (medium torque), and high-stiffness region (high torque), respectively (recall Fig. 11).

The results in Fig. 15 show that the gain-scheduled controller (in blue) yields the most consistent results, being neither under- or overdamped at any torque/stiffness range. In contrast, both linear controllers are either underdamped (high stiffness controller (yellow) at low torque), or overdamped (low stiffness controller (red) at high torque). In the middle range the gain-scheduled controller outperforms both. Notice that in the higher stiffness region (Fig. 15c), the system demonstrates an approx. 75% lower rise and settling time compared to the low stiffness region, indicating an increase in bandwidth which is available to be exploited.

B. Plant comparison: Torque tracking and Transparency

Next we compare SEAs based on the non-linear elastic element to two linear SEAs with stiffness values at the extremes of the non-linear element (30 and 300 Nm/rad). All plants are commanded a reference sine sweep with 1 Nm amplitude and offset $\tau_{\text{offset}} \in \{0, 9\}$ Nm. This offset places the non-linear element in either its low- or high-stiffness operating range. We then compute frequency response.

Fixed-output torque tracking results are shown in Fig. 16. The non-linear plant does show a significant shift as a result of its different operating point. At $\tau_{\text{offset}} = 0$ Nm, its stiffness is nearly identical to that of the low stiffness plant, and thus it yields a nearly identical response (red and blue lines). Conversely, at $\tau_{\text{offset}} = 9$ Nm, its stiffness increases to approx. 220 Nm/rad and thus its response approaches that of the high stiffness plant (yellow lines). Bandwidth as measured by -3 dB point increases from 5.5 Hz to 11.5 Hz for $\tau_{\text{offset}} \in \{0, 9\}$ Nm, respectively.

Transparency can be measured by the torque tracking error as function of output motion: we impose a sinusoidal load velocity sweep, while setting a constant torque reference $\tau^* \in \{0, 9\}$ Nm. Again, this places the non-linear elastic element in different stiffness operating regions. Fig. 17 shows the resulting torque error as function of $\dot{q}$. As with the torque tracking results, the non-linear plant approaches the low-stiffness plant behaviour at $\tau^* = 0$ Nm and the high-stiffness plant behaviour at $\tau^* = 9$ Nm, respectively. In other words, it achieves similar high transparency as the low-stiffness plant.

The torque tracking and transparency results can be summarised as follows: The non-linear series elastic actuator offers the transparency advantages of a low-stiffness actuator at low load levels, and the high torque tracking bandwidth of a high-stiffness actuator at high loads.

VI. Experimental results

This section presents preliminary results of the prototype in closed-loop force control. The motor was current controlled by an ODrive motor controller[8], with setpoints being sent by the Frdm K64F running the torque controller at 200 Hz. Ground truth torque measurements are provided by

[5]Maxon EC60 flat, 614949, 200 W, 536 mNm continuous torque.
[6]Maxon MILE encoder, 651168, 4096 CPT.
[7]Maxon GP52C, 223089, 43:1 reduction, 30 Nm continuous torque.
[8]ODrive Robotics, *ODrive v3.6*.

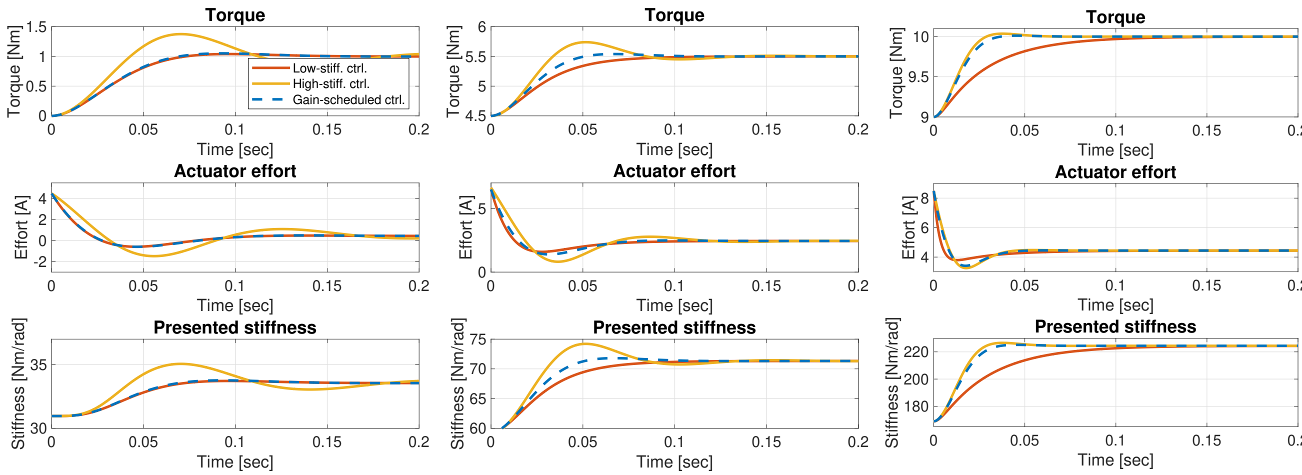

(a) Step from 0 to 1 Nm torque. **(b)** Step from 4.5 to 5.5 Nm torque. **(c)** Step from 9 to 10 Nm torque.

Fig. 15: Simulation: Step response of the non-linear plant at different torque/stiffness ranges, comparing different controllers.

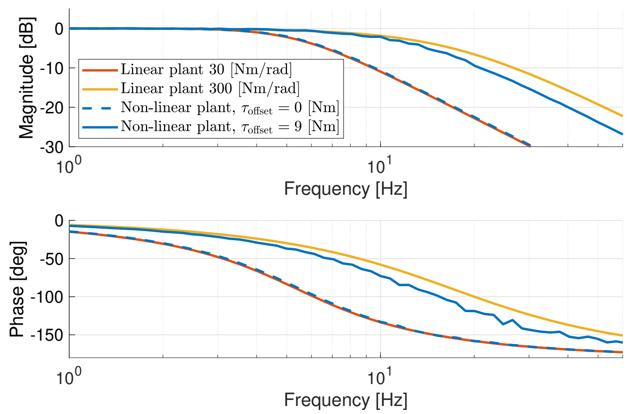

Fig. 16: Simulation: Torque tracking frequency response.

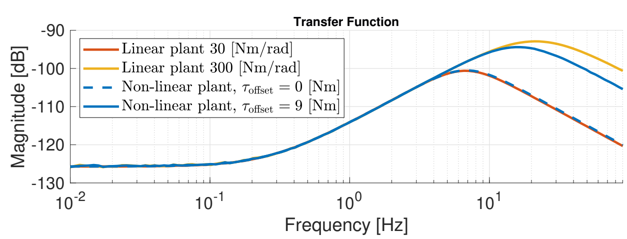

Fig. 17: Simulation: Transparency frequency response.

the ATI Mini-40. Step responses are shown in different parts of the stiffness range, demonstrating control performance despite varying stiffness.

Fig. 18 shows experimental step responses between -4, 0, and 4 Nm setpoints (in the 40-60 Nm/rad range cf. Fig. 11, and limited by the range of the ATI F/T sensor). The top plots show both the torque estimated based on deflection, and the ground-truth FT sensor measurement, which correspond well overall. The deflection settles rapidly, with settling times in the range 70-110 ms, which is comparable to simulation results for this part of the stiffness range. In the step from 4 to -4 Nm however, some oscillatory behaviour can be observed, which we attribute to mechanical non-idealities with the prototype, and the relatively low sample frequency.

VII. Discussion

The non-linear elastic element prototype realised in this work demonstrates a peak torque of 10 Nm and base stiffness of 40 Nm/rad, in agreement with model predictions. The maximum stiffness however, is significantly lower. We attribute this mainly to (visible) structural deformation, resulting in non-tangential forces that do not contribute torque. This also produced some asymmetry in the torque/stiffness profiles around zero deflection, which we hope to solve in the next prototype. The deficiencies in the preliminary prototype were also visible in experimental results.

Comparing related work [18], the prototype produces 12x higher torque at approx. 3.6x the size and 4.2x higher mass, partly due to the use of stronger magnets and more effective magnet placement. Both this work and [18] show that magnetic repulsive force can be used for a viable nonlinear series elastic element.

VIII. Conclusion

In this work we developed a magnet-based progressive elastic element for use in progressive series-elastic actuators. A thorough analysis was presented, together with design guidelines, including an analytical model that uses empirical magnet data to predict the torque and stiffness curves of such elastic elements. It was shown to accurately predict the prototype's main characteristics, making it a suitable design tool.

A prototype was developed to validate the concept. The prototype achieves ±10 Nm torque and a stiffness range (min-max stiffness ratio) of 3x in experiment. This verified that the presented analytical model gives accurate predictions and is therefore a useful tool in the design of magnet-based non-linear series elastic actuators.

Finally, a gain-scheduled quadratic regulator controller was presented that outperforms linear controllers throughout

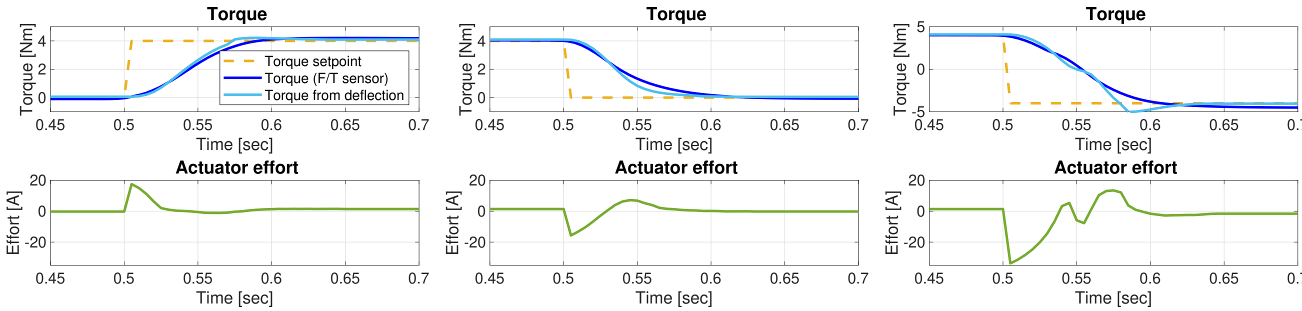

(a) From 0 to 4 Nm. **(b)** From 4 to 0 Nm. **(c)** From 4 to -4 Nm.

Fig. 18: Experiment: Step response between setpoints in different parts of the stiffness range.

the stiffness range, as shown in presented simulations. We believe an appropriate non-linear controller is essential to fully leverage the advantages of progressive stiffness. The controller was successfully applied to the developed prototype, with similar performance.

Progressive stiffness provides the transparency advantage of a low-stiffness actuator at low load levels, and high torque tracking bandwidth of a high-stiffness actuator at high loads. It also retains advantages compared to high-stiffness actuation that are not immediately visible in the data, including increased safety and higher torque resolution at lower loads. Additionally, compared to a linear low-stiffness actuator, it can achieve a larger peak torque for a given maximum deflection.

We suggest a few directions for future work. First, to solve drawbacks of the current prototype, subsequent prototypes should be manufactured using stiffer materials, such as composites, aluminium, or non-magnetic steel. Second, designs with arc magnets should be developed, as they should offer far superior torque and stiffness density.

References

[1] G. Pratt and M. Williamson, "Series elastic actuators," *IEEE/RSJ International Conference on Intelligent Robots and Systems (IROS)*, 1995.

[2] G. A. Pratt, M. M. Williamson, P. Dillworth, J. Pratt, and A. Wright, "Stiffness isn't everything," *Experimental Robotics IV Lecture Notes in Control and Information Sciences*, 253–262, 1995.

[3] W. Roozing, J. Malzahn, N. Kashiri, D. G. Caldwell, and N. G. Tsagarakis, "On the stiffness selection for torque-controlled series-elastic actuators," *IEEE Robotics and Automation Letters*, vol. 2, no. 4, 2255–2262, 2017.

[4] D. Robinson, J. Pratt, D. Paluska, and G. Pratt, "Series elastic actuator development for a biomimetic walking robot," *IEEE/ASME International Conference on Advanced Intelligent Mechatronics (AIM)*, 1999.

[5] B. Vanderborght *et al.*, "Variable impedance actuators: Moving the robots of tomorrow," *IEEE/RSJ International Conference on Intelligent Robots and Systems (IROS)*, pp. 5454–5455, 2012.

[6] S. Wolf *et al.*, "Variable stiffness actuators: Review on design and components," *IEEE/ASME Transactions on Mechatronics*, vol. 21, no. 5, pp. 2418–2430, 2016.

[7] I. Thorson and D. Caldwell, "A nonlinear series elastic actuator for highly dynamic motions," *IEEE/RSJ International Conference on Intelligent Robots and Systems (IROS)*, 2011.

[8] A. Schepelmann, K. A. Geberth, and H. Geyer, "Compact nonlinear springs with user defined torque-deflection profiles for series elastic actuators," *IEEE International Conference on Robotics and Automation (ICRA)*, 2014.

[9] N. Schmit and M. Okada, "Design and realization of a non-circular cable spool to synthesize a nonlinear rotational spring," *Advanced Robotics*, vol. 26, no. 3-4, 234–251, 2012.

[10] J. Realmuto, G. Klute, and S. Devasia, "Nonlinear passive cam-based springs for powered ankle prostheses," *Journal of Medical Devices*, vol. 9, no. 1, 2015.

[11] J. Austin, A. Schepelmann, and H. Geyer, "Control and evaluation of series elastic actuators with nonlinear rubber springs," *IEEE/RSJ International Conference on Intelligent Robots and Systems (IROS)*, 2015.

[12] E. Barrett, J. Malzahn, and N. Tsagarakis, "A compliant mechanism with progressive stiffness for robotic actuation," *IEEE/ASME International Conference on Advanced Intelligent Mechatronics (AIM)*, 2021.

[13] J. Malzahn, E. Barrett, and N. Tsagarakis, "A rolling flexure mechanism for progressive stiffness actuators," *IEEE International Conference on Robotics and Automation (ICRA)*, 2019.

[14] C. Jarrett and A. McDaid, "Modeling and feasibility of an elastomer-based series elastic actuator as a haptic interaction sensor for exoskeleton robotics," *IEEE/ASME Transactions on Mechatronics*, vol. 24, no. 3, pp. 1325–1333, 2019.

[15] D.-H. Kim and J.-H. Oh, "Hysteresis modeling for torque control of an elastomer series elastic actuator," *IEEE/ASME Transactions on Mechatronics*, vol. 24, no. 3, pp. 1316–1324, 2019.

[16] A. Sudano, D. Accoto, L. Zollo, and E. Guglielmelli, "Design, development and scaling analysis of a variable stiffness magnetic torsion spring," *International Journal of Advanced Robotic Systems*, vol. 10, no. 10, p. 372, 2013.

[17] A. H. Memar, N. Mastronarde, and E. T. Esfahani, "Design of a novel variable stiffness gripper using permanent magnets," in *2017 IEEE International Conference on Robotics and Automation (ICRA)*, Singapore, Singapore: IEEE, 2017, pp. 2818–2823.

[18] F. Rafeedi, J. H. Yoon, and D. Hong, "Design and control of a novel compact nonlinear rotary magnetic SEA (MSEA) for practical robotic gripper implementation," *IEEE Robotics and Automation Letters*, pp. 7643–7650, 2021.

[19] I. Hunter and S. Lafontaine, "A comparison of muscle with artificial actuators," *Technical Digest IEEE Solid-State Sensor and Actuator Workshop*, 178–185, 1992.

[20] G. C. Joyce, P. M. Rack, and D. R. Westbury, "The mechanical properties of cat soleus muscle during controlled lengthening and shortening movements," *The Journal of Physiology*, vol. 204, no. 2, 461–474, 1969.